Coupled Excited States in Nickel(II) Complexes Probed by Polarized Absorption Spectroscopy

Guillaume Bussière and Christian Reber*

Contribution from the Département de chimie, Université de Montréal, Montréal QC H3C 3J7, Canada

Received December 1, 1997

Abstract: The absorption spectra of $Ni(H_2O)_6^{2+}$, *trans*-$NiCl_2(H_2O)_4$, and $NiCl_6^{4-}$ show an unusual band shape for the $^3A_{2g} \rightarrow {}^3T_{1g}$, ^1E_g (O_h labels) electronic transitions in the near-infrared to visible wavelength range. A barely resolved broad band and an intense vibronic progression with a spacing larger than the totally symmetric ground-state metal−ligand vibrational frequency are superposed. Low-temperature polarized spectra are analyzed with a quantitative model and both the large interval and the band intensities are shown to arise from efficient intersystem crossings between the two excited states. Alternative assignments proposed in the literature are examined.

Introduction

Interactions between multiple electronic states are of key importance to many areas of chemistry, such as electron-transfer processes and photochemical reactions.[1,2] Transition metal compounds are ideal model systems for an investigation of interacting states because of their rich electronic structure with excited-state energies and other properties that can be controlled by simple chemical modifications such as ligand substitutions. The high symmetry of these molecules imposes rigid group theoretical constraints, and crystal field theory can be used for a complete identification of all low-energy electronic states. Electronic spectroscopy provides the detailed experimental information needed for a complete characterization of the interaction between excited states of the title compounds.

We apply polarized absorption spectroscopy to single crystals of three hexacoordinated nickel(II) complexes with aquo and chloro ligands. The electronic spectra of such complexes have attracted much interest in the past.[3−8] Among their most unusual features is an intense vibronic progression on the high-energy side of a spin-allowed d−d band between approximately 500 and 1000 nm. Its spacing is significantly larger than the ground-state totally symmetric vibrational energy of all three complexes. We present a quantitative model to calculate the shape of the complete band system with its prominent vibronic structure, including the large spacing of the vibronic progression. Our analysis shows that the excited-state force constant of a bond is not the only factor determining the energy separation within a vibronic progression. The vibronic structure is also affected by the coupling between energetically close excited states, an effect neglected in conventional spectroscopic assignments, despite its important influence on properties and reactivities of excited states. In the title compounds, the interaction between states of identical symmetry is caused by spin−orbit coupling, and we derive and discuss its effects from quantitative calculations of the experimental absorption band shapes. Our time-dependent quantum mechanical model provides information on nonadiabatic transitions between coupled electronic states. Complexes with resolved d−d bands provide a unique opportunity to study such effects because the symmetry of all relevant states can be obtained from crystal field theory, leaving a very small number of adjustable parameters for the theoretical analysis. The influence of coupled excited states on spectra is not limited to crystal field bands, it is an effect that is important in the electronic spectroscopy of other classes of compounds and materials.

A number of models and assignments have been proposed for the spectroscopic region of interest,[3−6,8] the most recent being a refined crystal field approach to nickel complexes with nitrogen and sulfur donor ligands.[9] The main emphasis of most models is on purely electronic transition energies calculated from the energy differences between states in Tanabe−Sugano diagrams or from electronic structure calculations. Energies and intensities of vibronic bands and progressions have received less detailed attention. Our approach unifies these facets and identifies the spectroscopic manifestations of intersystem crossings. Literature models for the vibronic structure include proposals such as a two-phonon progression in a non totally symmetric mode to account for the unusual structure observed in hexacoordinated nickel(II) halides[10] or the textbook attribution of the double maximum in the region of interest of the absorption spectrum of $Ni(H_2O)_6^{2+}$ to a Jahn−Teller effect,[11] while another very recent textbook concludes that there is no agreed explanation for this splitting.[12] We comment on these interpretations and on the long-standing controversy on singlet and triplet assignments for transition metal complexes with strongly coupled electronic states.[3−6,8]

(1) Bernardi, F.; Olivucci, M.; Robb, M. A. *Chem. Soc. Rev.* **1996**, 322.
(2) Romstad, D.; Granucci, G.; Persico, M. *Chem. Phys.* **1997**, *219*, 21.
(3) Jørgensen, C. K. *Acta Chem. Scand.* **1955**, *9*, 405.
(4) Jørgensen, C. K. *Acta Chem. Scand.* **1955**, *9*, 1362.
(5) Pryce, M. H. L.; Agnetta, G.; Garofano, T.; Palma-Vittorelli, M. B.; Palma, M. U. *Philos. Mag.* **1964**, *10*, 77.
(6) Reedijk, J.; Van Leeuwen, P. W. N. M.; Groeneveld, W. L. *Rec. Trav. Chim. Pays-Bas* **1968**, *87*, 129.
(7) Ferguson, J. *Progr. Inorg. Chem.* **1970**, *12*, 159.
(8) Solomon, E. I.; Ballhausen, C. J. *Mol. Phys.* **1975**, *29*, 279.
(9) Stranger, R.; McMahon, K. L.; Gahan, L. R.; Bruce, J. I.; Hambley, T. W. *Inorg. Chem.* **1997**, *36*, 3466.
(10) Benedek, G.; Pollini, I.; Piseri, L.; Tubino, R. *Phys. Rev. B* **1979**, *20*, 4303.
(11) Lee, J. D. *Concise Inorganic Chemistry*, 4th ed.; Chapman and Hall: London, 1991; p 960.
(12) Kettle, S. F. A. *Physical Inorganic Chemistry*; University Science Books: Sausalito, 1996; p 175.

S0002-7863(97)04073-0 CCC: $15.00
Published on Web 06/14/1998

Experimental Section

Crystals of *trans*-$NiCl_2(H_2O)_4 \cdot 2H_2O$ and $Ni(H_2O)_6(NO_3)_2$ were obtained by slow evaporation of saturated aqueous solutions of $NiCl_2 \cdot 6H_2O$ (Fisher Chemicals) and $Ni(NO_3)_2 \cdot 6H_2O$ (Biopharm) over several days. Samples for spectroscopic measurements were obtained through several recrystallizations. Infrared spectra are in excellent agreement with the literature.[13] $NiCl_2(H_2O)_4 \cdot 2H_2O$ crystallizes as very regular monoclinic green prisms. The crystal structure shows only one site for the $NiCl_2(H_2O)_4$ complex.[14] The shortest separation between nickel centers is 6.5 Å without shared ligands or bridging water molecules. Larger metal−metal distances in this structure involve hydrogen bonds through at least one noncoordinated water molecule. The crystals used for spectroscopic measurements had clearly defined optical extinction directions, determined between crossed polarizers. The molecular Cl−Ni−Cl axis is parallel to the crystallographic *a* axis which coincides with the long side of the crystals and one of the extinction directions.[14] Spectra were measured with the incident light beam perpendicular to the crystal surface containing the *ab* plane. The $H_2O-Ni-OH_2$ bonds are nearly perpendicular to the *a* axis in this arrangement. These crystals allow us therefore to measure spectra polarized along molecular axes.

$Ni(H_2O)_6(NO_3)_2$ crystallizes as blue-green triclinic crystals with less clearly defined extinction directions than $NiCl_2(H_2O)_4 \cdot 2H_2O$. Crystals were obtained from saturated aqueous solutions of $Ni(NO_3)_2 \cdot 6H_2O$ (Biopharm) within several days. The crystal structure of this compound again shows only one site for the Ni^{2+} ion,[15] but the molecular axes do not coincide with the extinction directions.

The crystal growth and near-infrared spectroscopic properties of $CsMgCl_3:Ni^{2+}$ were described previously.[16] In the following we analyze the absorption spectrum of a crystal used for the luminescence study in the literature.[16]

Crystal thicknesses for absorption spectroscopy were between 0.5 and 1 mm. Low-temperature polarized spectra were measured with a Varian Cary 5E spectrometer equipped with a pair of Glan-Taylor polarizers. All spectra are corrected for the baseline of the instrument. The sample temperature was controlled with an Oxford Instruments CF-1204 helium gas flow cryostat. Raman spectra were measured using the 488.0-nm blue line of a Coherent Innova 90−5 argon ion laser and a Spex 14018 monochromator with a photomultiplier (Hamamatsu R955) and a photon counting system (Spex DPC-2).

Spectroscopic Results

All three nickel(II) complexes show NIR−VIS absorption spectra with three spin-allowed transitions, as illustrated for $Ni(H_2O)_6^{2+}$ in Figure 1, where the bands are assigned in O_h symmetry. In the following, we focus on the region of the lowest-energy singlet−triplet intersection, involving the $^3T_{1g}(^3F)$ and ^1E_g excited states in the energy range of the middle spin-allowed band in the spectrum of Figure 1. This region is denoted by the dotted rectangle in the figure.

The polarized single-crystal absorption spectra for *trans*-$NiCl_2(H_2O)_4 \cdot 2H_2O$ in the region of the $^3A_{2g} \rightarrow {}^3T_{1g}(^3F),{}^1E_g$ transitions (O_h labels) are shown in Figure 2. The electronic transitions from the ground state to both excited states are parity-forbidden and the oscillator strength in the wavelength range shown in Figure 2 is on the order of 5×10^{-6}, typical for this type of transitions. The oscillator strength increases by 27% between 5 and 300 K. The temperature dependence of the spectrum does not provide evidence for structural phase transitions. A simple paramagnetic behavior is observed at temperatures down to 5 K, ruling out cooperative electronic excitations in our spectra.[17] The band system in the near-infrared to visible (NIR/VIS) range extends from approximately 12000 to 18000 cm^{-1} and consists of a broad band and an intense vibronic progression. The maxima of the broad band are at 13240 and 13430 cm^{-1} in σ and π polarization, respectively. Weak vibronic structure on the broad band is observed in both polarizations with an average spacing of 357 cm^{-1}, indicated schematically in Figure 2. The intense vibronic progression has its first maximum at 14780 cm^{-1} in σ polarization. The members of the progression in the σ-polarized spectrum are separated by 430 ± 5 cm^{-1}, as marked in Figure

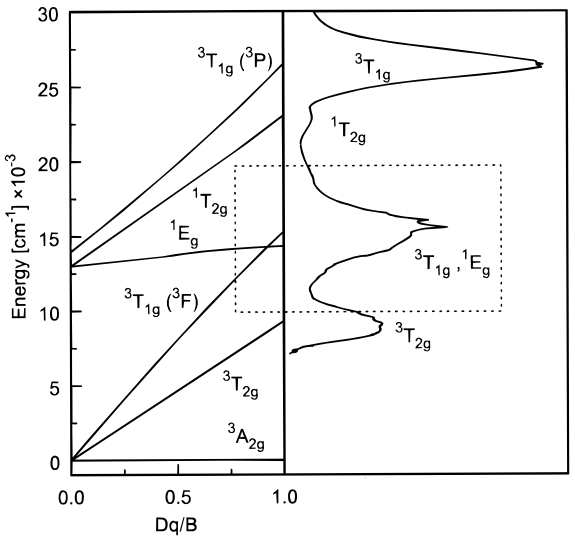

Figure 1. Overview absorption spectrum and band assignments for $Ni(H_2O)_6^{2+}$. The unpolarized experimental spectrum of $Ni(H_2O)_6(NO_3)_2$ was measured at 5 K and is identical to the literature data.[8] The dotted rectangle denotes the region of the first singlet−triplet intersection, shown in more detail in Figures 2, 4, and 5 for all compounds studied.

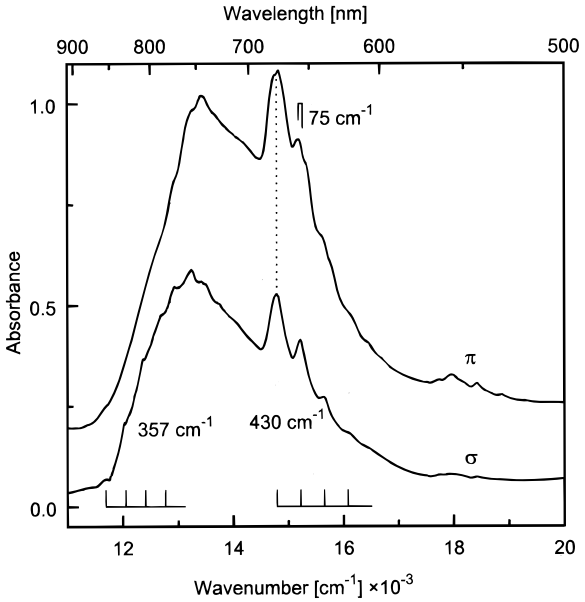

Figure 2. Polarized absorption spectra of *trans*-$NiCl_2(H_2O)_4 \cdot 2H_2O$ at 5 K in the region of the $^3A_{2g}$, ^3E_g and $^1A_{1g}$, $^1B_{1g}$ bands (D_{4h} labels). Polarization directions are given relative to the molecular Cl−Ni−Cl axis. The main vibronic progressions are indicated for the σ-polarized spectrum. The π-polarized spectrum is offset by 0.15 absorbance units for clarity.

(13) Adams, D. M.; Lock, P. J. *J. Chem. Soc. A* **1971**, 2801.
(14) Mizuno, J. *J. Phys. Soc. Jpn.* **1961**, *16*, 1574.
(15) Bigoli, F.; Braibanti, A.; Tiripicchio, A.; Tiripicchio, C. *Acta Crystallogr.* **1971**, *B27*, 1427.
(16) Reber, C.; Güdel, H. U. *Inorg. Chem.* **1986**, *25*, 1196.
(17) Haseda, T.; Kobayashi, H.; Date, M. *J. Phys. Soc. Jpn.* **1959**, *14*, 1724.

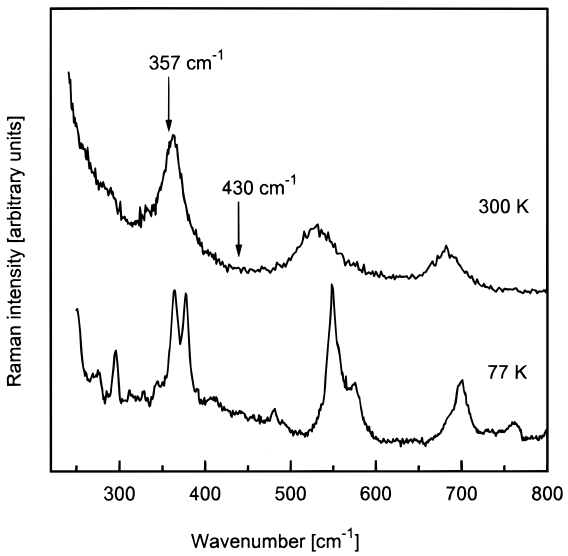

Figure 3. Unpolarized Raman spectra of *trans*-$NiCl_2(H_2O)_4 \cdot 2H_2O$. The arrows indicate the average spacing of the vibronic progressions in the absorption spectra of Figure 2.

2. The π-polarized spectrum shows two very similar 430 cm^{-1} progressions with an average separation of 75 cm^{-1} between corresponding maxima, indicated in Figure 2 for the second member of both progressions. The lowest energy maximum of the first progression is at 14 760 cm^{-1}, overlapping the corresponding maximum of the higher energy progression at 14 830 cm^{-1}. The progression in σ polarization has its maxima at energies close to the first progression in π polarization, as illustrated by the dotted line in Figure 2. The weak vibronic peaks at approximately 18 000 cm^{-1} involve vibrational modes of the aquo ligands.[8]

The Raman spectra of $NiCl_2(H_2O)_4 \cdot 2H_2O$ are shown in Figure 3 at room temperature and at 77 K. The vibrational energies are very similar at both temperatures, again indicating negligible structural changes of the chromophores as a function of temperature. Vibrational energies at 77 K are 532, 377, and 364 cm^{-1}. The signal at 364 cm^{-1} in the room temperature spectrum is attributed to the totally symmetric Ni−H_2O stretching mode based on its polarization and on literature assignments.[13] We note that there is no Raman signal corresponding to the spacing of 430 cm^{-1} in the intense vibronic progression observed in the absorption spectra of Figure 2.

Our polarized single-crystal absorption spectra of $Ni(H_2O)_6(NO_3)_2$ are identical to the literature spectra for this compound[8] and similar to the data reported for $Ni(H_2O)_6^{2+}$ in a variety of crystals and glasses.[3,6,8] An intense vibronic progression with a spacing of 490 ± 20 cm^{-1} is observed on the high-energy side of the broad band. The totally symmetric vibrational mode has a Raman frequency of 397 cm^{-1}, again lower in energy than the spacing of the intense vibronic progression. The average spacing of the resolved progression on the broad band is 355 cm^{-1} and the oscillator strength of the band system increases by 24% between 5 K and room temperature. The overall absorption spectrum is shown in Figure 1 and the region of interest is compared to our theoretical model in Figure 4.

The absorption spectrum of $CsMgCl_3$:Ni^{2+} is identical to the literature spectra[18,19] and it is compared to our theoretical model in Figure 5b. The band intensity increases by 30% between 15 K and room temperature. The broad band shows weak vibronic structure with an average spacing of 240 cm^{-1}. The spacing of the intense progression is 300 cm^{-1}, again higher than the a_{1g} vibrational frequency of 255 cm^{-1}.[20] Similar spectra are obtained for pure crystalline $CsNiCl_3$ and $CsNiBr_3$, with additional fine structure at low temperature due to magnetic ordering.[19]

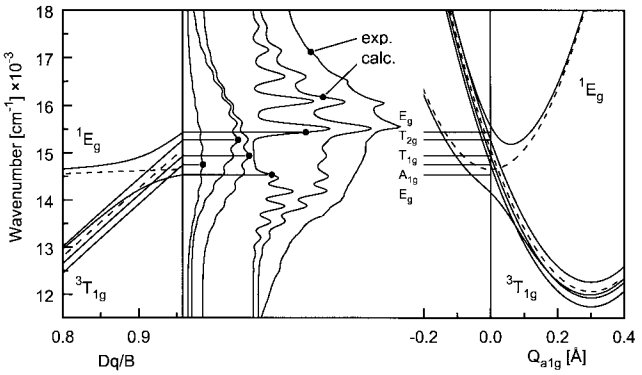

Figure 4. Crystal field states (left-hand panel) and potential energy surfaces (right-hand panel) for an octahedral complex of nickel(II) in the $^3T_{1g}/^1E_g$ energy range. Calculated spectra for the transition to each electronic state are shown in the central panel. Lines with markers connect electronic states and their corresponding calculated spectra. The total calculated spectrum (calc.) is obtained as the sum of the four individual spectra and is compared to the experimental spectrum of $Ni(H_2O)_6^{2+}$ measured at 5 K.

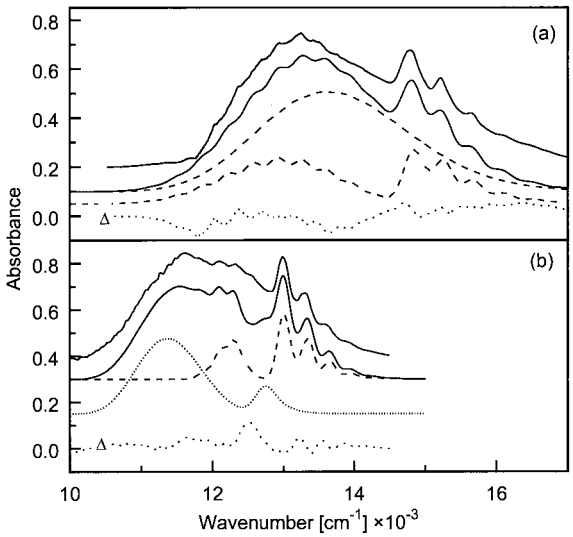

Figure 5. (a) Calculated and experimental absorption spectra for *trans*-$NiCl_2(H_2O)_4 \cdot 2H_2O$ in σ polarization. The top trace (solid line) denotes the experimental spectrum, followed by the total calculated spectrum (solid line) separated from the experimental spectrum by 0.1 absorbance units for clarity. The two dotted traces denote the calculated spectra for the E_g and the coupled A_{1g} levels arising from $^3A_{2g}$ and $^1A_{1g}$. The difference trace between experimental and calculated spectra is denoted by Δ. (b) Calculated and experimental absorption spectra of $CsMgCl_3$:Ni^{2+} in σ polarization. The top trace (solid line) denotes the experimental spectrum, followed by the total calculated spectrum (solid line), separated from the experimental spectrum by 0.1 absorbance units. The calculated spectra for two sets of coupled E_g levels are represented by dotted lines. The difference trace between experimental and calculated spectra is denoted by Δ.

Discussion

We combine absorption energies and intensities, vibrational spectra, and electronic states derived from crystal field theory

(18) McPherson, G. L.; Stucky, G. D. *J. Chem. Phys.* **1972**, *57*, 3780.
(19) Ackerman, J.; Holt, E. M.; Holt, S. L. *J. Sol. State Chem.* **1974**, *9*, 279.
(20) Johnstone, I. W.; Jones, G. D.; Lockwood, D. J. *Solid State Commun.* **1981**, *39*, 395.

Table 1. Spectroscopic Parameters for the Ground (g.s) and Excited (e.s.) Electronic States

parameter	$Ni(H_2O)_6^{2+}$	$NiCl_2(H_2O)_4$	$NiCl_6^{4-}$
$^3\Gamma$ origins (cm^{-1})	12066 E_g ($^3T_{1g}$)[a] 11737 A_{1g} ($^3T_{1g}$)[a] 11925 T_{1g} ($^3T_{1g}$)[a] 12260 T_{2g} ($^3T_{1g}$)[a]	10365 A_{1g} ($^3A_{2g}$) 10500 E_g ($^3A_{2g}$)	10400 E_g (^3E_g) 10700 E_g (^3E_g) 11000 A_{1g} (^3E_g) 11200 A_{2g} (^3E_g) 11850 E_g ($^3A_{2g}$) 12100 A_{1g} ($^3A_{2g}$)
$^1\Gamma$ origin (cm^{-1})	14651 E_g (^1E_g)[a]	14403 A_{1g} ($^1A_{1g}$)	12500 E_g (^1E_g)
vibrational frequencies (cm^{-1})			
$h\omega_{a1g}$, g.s.	397	364	255
$h\omega_T$, $^3\Gamma$ e.s.	355	357	240
$h\omega_S$,$^1\Gamma$ e.s.	397	364	255
potential minima (Å)			
ΔQ_T, $^3\Gamma$ e.s.	0.30	0.295	0.17
ΔQ_S, $^1\Gamma$ e.s.	0.00	0.05	0.00
coupling constant V_{ST} (cm^{-1})	661	730	350
damping factor Γ (cm^{-1})	60	100	60
transition dipole moments, μ_S/μ_T	0.00/1.00	0.09/0.91	0.00/1.00

[a] Calculated with $Dq = 910.7$ cm^{-1}, $B = 950$ cm^{-1}, $C/B = 4$, $\lambda = -270$ cm^{-1} ($\lambda = 0$ for E_g levels);[22] crystal field triplet levels correspond to absorption maxima and are higher by 3013 cm^{-1} than the band origins given in the table.

Scheme 1. Electronic States Involved in the Absorption Bands in the Region of the First Singlet−Triplet Intersection for Octahedral, Tetragonal, and Trigonal Complexes of Nickel(II)[a]

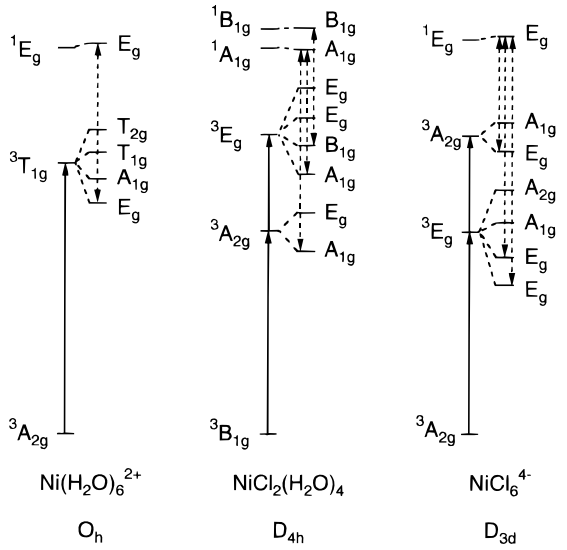

[a] The energetic order of triplet states and their spin−orbit sublevels is discussed in the text. Solid arrows denote spin-allowed absorption transitions. Dotted arrows connect pairs of interacting levels.

to fully analyze the NIR/VIS band system for nickel(II) complexes with three different point group symmetries. Idealized O_h and D_{4h} point groups are used for $Ni(H_2O)_6^{2+}$ and $NiCl_2(H_2O)_4$, respectively. The Ni^{2+} centers doped into $CsMgCl_3$ occupy a site with exact D_{3d} symmetry. All crystal field states of interest can be derived from the relevant character tables[21] and are summarized in Scheme 1. Octahedral (O_h) symmetry corresponds to the simplest situation with only one pair of interacting singlet and triplet levels. These two levels have E_g symmetry and are connected by the dotted arrows in Scheme 1. Tetragonal (D_{4h}) symmetry offers two singlet states that can interact with one or two triplet states, and in trigonal (D_{3d}) symmetry we probe one singlet state interacting with several triplets at different energies. All pairs of interacting levels are indicated in Scheme 1. These pairs of coupled levels with their potential energy surfaces along a totally symmetric normal coordinate are the key aspect accounting for the unusually large vibronic spacings in the absorption spectra. The quantitative potential energy surfaces for the coupled states are used to calculate absorption spectra using time-dependent theory, an approach that allows us to visualize the vibronic dynamics involving the coupled states and their spectroscopic consequences. The spectroscopic features observed in the three different symmetries will be unified with the model approach presented in the following. We will then briefly compare our analysis to several alternative assignments presented in the literature.

$Ni(H_2O)_6^{2+}$: O_h Symmetry, One Singlet−Triplet Interaction. The quantitative analysis of this band shape proceeds through three main stages: first, the electronic states with their potential energy surfaces have to be defined, then the most efficient intensity mechanism for the transitions has to be determined, and finally the resulting band shapes have to be calculated. These three stages will be discussed in detail for $Ni(H_2O)_6^{2+}$, an analogous approach is then applied to $NiCl_2(H_2O)_4$ and $NiCl_6^{4-}$. Crystal field theory can be used to quantitatively define the energies of all electronic states for this complex in the NIR/VIS region. The parameters B and Dq were determined from the three spin-allowed absorption bands of this complex[6] and the literature value of -270 cm^{-1} for the spin−orbit coupling constant λ determined from EPR spectroscopy was used.[22] The energies of the relevant electronic states are calculated with these crystal field parameters and given in Table 1. Figure 4 summarizes our model and its comparison with the experimental absorption spectrum of $Ni(H_2O)_6^{2+}$. The left-hand panel of the figure illustrates the crossing region between the ^1E_g and $^3T_{1g}(^3F)$ levels as a function of the ratio Dq/B and is identical to a standard Tanabe-Sugano diagram for the two excited states of interest. The dotted lines indicate the singlet−triplet crossing in the absence of spin−orbit coupling, as shown in Figure 1. The highest value of Dq/B shown in Figure 4 corresponds to the crystal field parameters in Table 1. The energetic order of the spin−orbit levels at this abscissa value is identical to Scheme 1 and given in the middle panel of Figure 4. The avoided crossing between the E_g levels arising from the singlet and triplet excited states is caused by the off-diagonal matrix element for spin−orbit coupling between the $E_g(^3T_{1g})$ and $E_g(^1E_g)$ states, given as $-\sqrt{6}\lambda$ in the literature.[23] This

(21) Salthouse, J. A.; Ware, M. J. *Point group character tables and related data*; Cambridge University Press: New York, 1972.

(22) Abragam, A.; Bleaney, B. *Electron Paramagnetic Resonance of Transition Metal Ions*; Clarendon Press: Oxford, 1970; p 451.

model applies to a complex with a rigid geometry corresponding to the ground-state molecular structure and does not include vibronic effects.

A physically more meaningful description of the electronic states includes vibronic effects and requires potential energy surfaces. We limit our analysis to one-dimensional harmonic surfaces along the totally symmetric normal coordinate of the metal−ligand breathing mode Q_{a1g}, as shown on the right-hand side of Figure 4 for all singlet and triplet excited states given in Scheme 1. The minimum of the ground-state surface defines the origin of the Q_{a1g} axis. The ^1E_g excited-state potential has its minimum also at $Q_{a1g} = 0$ because it arises from the same $t_{2g}^6e_g^2$ electron configuration as the ground state. The $^3T_{1g}$ excited state is expected to have its minimum at $Q_{a1g} > 0$, a consequence of the increased antibonding character of its $t_{2g}^5e_g^3$ electron configuration. This offset and the resulting Ni−H_2O bond elongations are assumed to be identical for all four spin−orbit levels arising from the $^3T_{1g}$ excited state. Spectroscopic data and calculated crystal field levels quantitatively define the potential energy surfaces for $Ni(H_2O)_6^{2+}$ with the parameter values summarized in Table 1. The frequency of the a_{1g} mode in the Raman spectrum of $Ni(H_2O)_6^{2+}$ is used to determine the harmonic potential energy surfaces for both the $^3A_{2g}$ and ^1E_g states. The vibrational frequency for the $^3T_{1g}$ excited state is lower than for the ground state, and we use the frequency of 355 cm^{-1} from the resolved vibronic structure of the $^3T_{1g}$ band, a value in close agreement with the literature.[8] This vibrational energy is used for all four potential energy surfaces arising from the $^3T_{1g}$ state.

The potential energy surfaces for the coupled E_g states are represented by the matrix:

$$V_{E_g} = \begin{pmatrix} \frac{1}{2}k_S(Q_{a1g} - \Delta Q_S)^2 + \Delta E_{ST} & V_{ST} \\ V_{ST} & \frac{1}{2}k_T(Q_{a1g} - \Delta Q_T)^2 \end{pmatrix} \quad (1)$$

The diagonal elements correspond to the harmonic (diabatic) excited-state potentials shown as dotted lines on the right-hand side of Figure 4, the diagonalized matrix defines the adiabatic potentials, shown as solid lines in the Figure. The indices S and T refer to singlet and triplet excited states, respectively, whose force constants $k_{S,T}$ are obtained from the vibrational frequencies given in Table 1. ΔE_{ST} denotes the energy difference between the origins of the transitions to coupled states of identical symmetry, given in Table 1. The coupling constant V_{ST} is set to the off-diagonal matrix element between the two E_g states, $-\sqrt{6}\lambda$,[23] using the numerical value of -270 cm^{-1} for λ, the ground-state spin−orbit coupling constant[22] to obtain the coupling constant V_{ST} in Table 1. The offset ΔQ_T is assumed to be identical for all triplet states and is the only unknown model parameter.

The dominant contribution to the experimental oscillator strengths for the centrosymmetric complexes studied occurs via a vibronically induced electric dipole mechanism, illustrated by the magnitude and temperature dependence of the oscillator strength. The observed bands are therefore based on vibronic origins involving ungerade parity enabling modes onto which all progressions in totally symmetric modes are built. We base our model on a single effective vibronic origin offset by the same energy from the electronic origin for transitions to all four states arising from $^3T_{1g}$ and we neglect magnetic dipole progressions built directly on the electronic origins. The intensity distributions within a progression built on an electronic origin and on a corresponding vibronic origin are reported to be identical for a large number of transition metal compounds with resolved electronic spectra.[24] We assume that this is also the case for the title compounds. The energies of the effective vibronic origins are given in Table 1. The experimental bandwidths of the individual vibronic transitions in our spectra are too large to allow us to distinguish between several different vibronic origins, in contrast to a comprehensive literature study on $Ni(H_2O)_6^{2+}$,[8] where two vibronic origins separated by 196 cm^{-1} were identified from a single-crystal spectrum.

We use the time-dependent theory of electronic spectroscopy to calculate absorption spectra.[25] Its application to transition metal compounds has been discussed in detail previously.[26,27] The absorption spectrum is given by

$$I(\omega) = C\omega \int_{-\infty}^{+\infty} e^{i\omega t}\{\langle\phi|\phi(t)\rangle e^{-\Gamma^2t^2 + [(iE_0)/\hbar]t}\}dt \quad (2)$$

with $I(\omega)$ denoting the intensity at frequency ω in arbitrary units, E_0 the energy of the vibronic origin, and Γ a phenomenological damping factor, determined from the width of each band forming the vibronic structure. Equation 2 was used to calculate the spectra arising from the transitions to the A_{1g}, T_{1g}, T_{2g}, and the coupled E_g levels in $Ni(H_2O)_6^{2+}$.

The most important ingredient to eq 2 is $\langle\phi|\phi(t)\rangle$ the autocorrelation function of a wave packet ϕ prepared on the potential energy surfaces of the final states at time $t = 0$ in the course of the electronic transition. We assume transition dipole moments that are constant along Q_{a1g} and identical for all levels arising from the triplet excited state. The quantity ϕ in eq 2 corresponds therefore to the lowest energy vibrational eigenfunction χ of the electronic ground state. The time-dependent wave function $\phi(t)$ is obtained with a split-operator algorithm[28] adapted to calculate wave packet dynamics on one or two final electronic states.[29−31]

The coupled potential surfaces in eq 1 are used to calculate $\phi(t)$ for the E_g states. The time-dependent wave function is a vector quantity with two components, corresponding to the states of singlet and triplet parentage. The initial wave function ϕ is given by

$$\phi = \begin{pmatrix} \phi_S(t=0) \\ \phi_T(t=0) \end{pmatrix} = \begin{pmatrix} \mu_S\chi \\ \mu_T\chi \end{pmatrix} \quad (3)$$

with μ_S and μ_T denoting the dipole moments for the transitions to singlet and triplet excited states, respectively. In our model for $Ni(H_2O)_6^{2+}$ we use $\mu_T = 1$ for all triplet levels and set μ_S to zero, giving no intensity to the spin forbidden band in the absence of spin−orbit coupling. The intensity of the transition to the ^1E_g excited state is therefore entirely borrowed from the $^3T_{1g}$ band.

We calculate the total spectrum as a superposition of individual spectra for each of the A_{1g}, T_{1g}, and T_{2g} levels with relative intensities of 1:3:3 based on the degeneracies of the

(23) Griffith, J. S. *The Theory of Transition Metal Ions*; Cambridge University Press: New York, 1961; p 307.

(24) Flint, C. D. *Coord. Chem. Rev.* **1974**, *14*, 47.
(25) Heller, E. J. *Acc. Chem. Res.* **1981**, *14*, 368.
(26) Zink, J. I.; Kim Shin, K.-S. In *Adv. Photochem.;* Volman, D. H., Hammond, G. S., Neckers, D. C., Ed.; John Wiley: New York, 1991; Vol. 16, p 119.
(27) Reber, C.; Zink, J. I. *Comments Inorg. Chem.* **1992**, *13*, 177.
(28) Feit, M. D.; Fleck, J. A., Jr.; Steiger, A. *J. Comput. Phys.* **1982**, *47*, 412.
(29) Alvarellos, J.; Metiu, H. *J. Chem. Phys.* **1988**, *88*, 4957.
(30) Jiang, X.-P.; Heather, R.; Metiu, H. *J. Chem. Phys.* **1989**, *90*, 2555.
(31) Engel, V.; Schinke, R.; Hennig, S.; Metiu, H. *J. Chem. Phys.* **1990**, *92*, 1.

final states, as suggested for $Ni(H_2O)_6^{2+}$ in the literature.[5,8] These three spectra are shown on the left-hand side of the central panel in Figure 4 and have their maxima at the calculated crystal field energies. The spectrum arising from the transition to the coupled E_g levels is given a relative intensity of 2, again assuming no intrinsic intensity for the $^3A_{2g} \rightarrow {}^1E_g$ transition, and it is added to the three Poisson bands for the transitions not involved in the singlet−triplet coupling. This total calculated spectrum and the experimental spectrum are shown as the two rightmost traces in the central panel to Figure 4. Their overall agreement is very good, especially considering that the model is based on an idealized point group and involves only a single adjustable parameter, ΔQ_T. We obtain a value of 0.30 Å for ΔQ_T, corresponding to an elongation of 0.12 Å for each $Ni^{2+}-H_2O$ bond. This value is within the typical range determined in the literature for large d−d bands[26] and similar to the value of approximately 0.1 Å given in a semiquantitative configurational coordinate diagram.[5] The calculated spacing between members of the progression on the high-energy side of the absorption band is 550 cm^{-1}, higher than the vibrational frequencies of all potential surfaces in the model calculation and in good agreement with the experimental separation of 490 cm^{-1}. To our knowledge this is the first *quantitative* calculation of both the energies and intensities of the vibronic structure for the $^3T_{1g}$ and ^1E_g excited states of $Ni(H_2O)_6^{2+}$.

The model in Figure 4 provides detailed insight on the singlet and triplet band assignments, which have caused some controversy in the literature.[3−6,8] The singlet and triplet characters of the coupled E_g levels can easily be calculated from the crystal field eigenfunctions. At the left-hand limit of the *Dq*/*B* abscissa the singlet character of the highest energy level, identified as ^1E_g, is 96%, the singlet character of the lower energy E_g level is only 4%. At the right-hand limit of the abscissa, the singlet character of the highest energy level decreases to 16%, the lower energy E_g level has singlet and triplet contributions of 83% and 17%, respectively. This electronic picture could lead us to attribute the lower energy band of the spectrum calculated for the coupled E_g states to the singlet and the higher energy band, which corresponds to the intense vibronic progression, to the triplet excited state. It is clear from the potential energy surfaces in Figure 4 that this assignment is not meaningful: the diabatic potential energy surface of the singlet excited state is placed higher in energy than the band assigned to the singlet based on electronic wave functions.

It is important to realize that all characterizations based on electronic wave functions apply to the rigid complex and implicitly involve the adiabatic approximation. Even in this approximation, the right-hand panel to Figure 4 provides a more complete picture: the singlet and triplet character varies as the complex moves along either the upper or lower adiabatic potential surface during a vibration. This variation is governed by the shapes and positions of the surfaces and the magnitude of the coupling constant V_{ST}, quantities that are only partially included in a purely electronic picture. Our analysis described in the preceding sections explicitly involves nonadiabatic transitions between the two surfaces, causing both the high intensity and the unusual vibronic splitting. The detailed spectra give therefore direct experimental information on the behavior of the complexes in coupled electronic states, a situation of current interest in photochemistry and molecular dynamics.[1,2]

Model calculations with inverted energetic order of the singlet and triplet diabatic potential energy surfaces did not lead to calculated spectra close to the experimental data, further corroborating our model analysis. Potential energy surfaces with minimum energies and positions similar to those in Figure 4 are also obtained for the following two compounds, where an automated and optimized search of parameter space was performed.

***trans*-$NiCl_2(H_2O)_4$: D_{4h} Symmetry, Two Different Singlets Coupled to Triplet States.** In this point group the ^1E_g (O_h) excited-state splits into $^1A_{1g}$ and $^1B_{1g}$ levels. The $^3T_{1g}$ state separates into $^3A_{2g}$ and ^3E_g, which are then further split by spin−orbit coupling, as illustrated in Scheme 1. The most important difference from O_h symmetry is that the $^3A_{2g}$ state can only interact with the $A_{1g}(^1A_{1g})$ state, whereas the ^3E_g state can couple to both $A_{1g}(^1A_{1g})$ and $B_{1g}(^1B_{1g})$.

The energetic order of triplet and singlet excited states in this tetragonal complex can be obtained from a crystal field calculation using the angular overlap formalism.[32,33] The angular overlap parameters $e_\sigma(H_2O)$ and $e_\pi(H_2O)$ of 4380 and 1000 cm^{-1} were determined from the spin-allowed band maxima of $Ni(H_2O)_6(NO_3)_2$ at 5 K. The corresponding absorption maxima of $NiCl_6^{4-}$ in $CsCdCl_3$,[34] $CsMgCl_3$,[18,19] and $NiCl_2$[10,35] were used to determine average values of 3700 and 990 cm^{-1} for $e_\sigma(Cl)$ and $e_\pi(Cl)$, respectively. These values were then transferred to the mixed-ligand complex $NiCl_2(H_2O)_4$. The Racah parameter *B* was set to 900 cm^{-1} (83% of the free ion value), the ratio *C*/*B* to 4 and the spin−orbit coupling constant ζ to 600 cm^{-1}. This calculation does not involve a fit, but it leads to spin-allowed band maxima for $NiCl_2(H_2O)_4$ in satisfactory agreement with the experimental values obtained at 5 K. The first band maximum is broad and located between 8100 and 8700 cm^{-1} (σ and π polarizations). It corresponds to the calculated maxima at 8114 and 9200 cm^{-1} for the barycenters of the ^3E_g and $^3B_{2g}$ excited states, respectively. The second band is observed at 13 240 cm^{-1} (σ) and 13 430 cm^{-1} (π) and calculated at 13 449 cm^{-1} ($^3A_{2g}(^3F)$) and 14 183 cm^{-1} ($^3E_g(^3F)$). The narrow third band maximum is observed at 24 300 cm^{-1} (σ and π), in good agreement with the calculated maxima at 24 692 cm^{-1} ($^3A_{2g}(^3P)$) and 25 258 cm^{-1} ($^3E_g(^3P)$).

The calculated energetic order of the excited states in the region of the NIR/VIS band system predicts the barycenter of the $^3A_{2g}$ state lower in energy by 735 cm^{-1} than the barycenter of the ^3E_g state. The $^1A_{1g}$ state is calculated at an energy lower by 178 cm^{-1} than the $^1B_{1g}$ state. This value compares favorably to the average separation of 75 cm^{-1} between the two progressions in the π-polarized absorption spectrum in Figure 2, especially since no angular overlap parameters were fitted to the spectrum of $NiCl_2(H_2O)_4$. This qualitative energetic order is given in Scheme 1 and confirmed in the following.

The experimental spectrum of *trans*-$NiCl_2(H_2O)_4$ shows a double progression in π polarization, but only the lower energy progression appears in σ polarization. The band maximum of the broad band in σ polarization is at lower energy than in π polarization. Transition energies and vibronic patterns can be combined with the calculated crystal field energies and indicate that the σ-polarized spectrum is dominated by the $^3B_{1g} \rightarrow {}^3A_{2g}$ band. This triplet excited state can only interact with the $^1A_{1g}$ state. The $^3B_{1g} \rightarrow {}^3E_g$ transition is expected at higher energy, as observed in π polarization. The ^3E_g state has A_{1g} and B_{1g} spin−orbit levels that can interact with both singlet excited states, leading to the two superposed progressions in the

(32) Larsen, E.; LaMar, G. N. *J. Chem. Educ.* **1974**, *51*, 633.
(33) Adamsky, H. *AOMX−an angular overlap program*; Institut für Theoretische Chemie, Heinrich-Heine-Universität Düsseldorf: Düsseldorf, Germany, 1995. The program is available at http://www.theochem.uni-duesseldorf.de/Computing/Progs/aomx/Welcome.html.
(34) Oetliker, U.; Riley, M. J.; Güdel, H. U. *J. Lumin.* **1995**, *63*, 63.
(35) Kozielski, M.; Pollini, I.; Spinolo, G. *J. Phys. C: Sol. Stat. Phys.* **1972**, *5*, 1253.

spectrum and confirming the energetic order derived from the angular overlap model. This experimental observation confirms that the singlet states gain most of their intensity from the triplet transitions, justifying the assumption made for the model in Figure 4.

The main contribution to the oscillator strength of the spectra in Figure 2 again arises from vibronic mechanisms involving ungerade parity enabling modes. These vibrational modes of $NiCl_2(H_2O)_4$ have been studied in detail,[13] and several e_u, a_{2u}, and b_{2u} vibrations with frequencies between 100 and 400 cm^{-1} are reported.[13] The oscillator strength of the spectra in Figure 2 is most likely built on such low-energy vibronic origins. Absorption and MCD spectra of octahedral $Ni(H_2O)_6^{2+}$ complexes with resolved vibronic origins show that t_{1u} modes are the most efficient enabling modes.[8] The t_{1u} mode splits into e_u and a_{2u} in the D_{4h} point group, indicating that b_{2u} modes are less important as enabling modes. We use group theoretical selection rules to examine the possible enabling modes for the spin allowed bands. In π polarization, the $^3B_{1g} \rightarrow {}^3E_g$ transition is only allowed with an e_u enabling mode and the $^3B_{1g} \rightarrow {}^3A_{2g}$ transition is not allowed with any of the ungerade parity enabling modes. The transition to the ^3E_g state therefore dominates the observed spectrum in π polarization and enabling modes of e_u symmetry are very efficient. In σ polarization, the $^3B_{1g} \rightarrow {}^3A_{2g}$ transition is allowed with e_u enabling modes, indicating that the experimental spectrum is dominated by this transition. The $^3B_{1g} \rightarrow {}^3E_g$ transition in σ polarization is allowed with a_{2u} or b_{2u} enabling modes which appear to be less efficient because no replica of the band shape observed in π polarization, involving only the ^3E_g state, can be observed in the σ-polarized spectrum of Figure 2. Both the group theoretical analysis of the observed polarizations and the comparison of calculated crystal field energy levels with experimental band maxima therefore confirm that the σ- and π-polarized spectra show predominantly the transitions to the $^3A_{2g}$ and ^3E_g states, respectively.

We use the same approach as presented for $Ni(H_2O)_6^{2+}$ in the preceding section, but we limit the calculation to the σ-polarized spectrum involving the $^3A_{2g}$ and $^1A_{1g}$ excited states. The model involves coupled A_{1g} surfaces and a simple harmonic surface for the E_g level of the $^3A_{2g}$ state, leading to a Poisson band shape. The intensity ratio of the two partial spectra is 1:2, again analogous to the calculation described for $Ni(H_2O)_6^{2+}$. The origins of the three transitions to singlet and triplet states, the offsets of the minima of both the triplet and singlet levels along Q_{a1g}, the vibrational frequency describing the harmonic potentials for the triplet excited states, the coupling constant V_{ST} and the transition moments μ_S and μ_T are all treated as adjustable parameters. We apply a simulated annealing technique to efficiently and systematically search this parameter space.[36] All parameters resulting from this refinement were obtained from several different sets of initial guesses using different annealing temperature profiles, indicating that the fit parameters are unique and correspond to the global minimum in parameter space. Their final numerical values are summarized in Table 1 and lead to a very good agreement between calculated and experimental spectra, as illustrated in Figure 5a. The calculated spacing within the intense progression is 420 cm^{-1}, in excellent agreement with the experimental spacing of 430 cm^{-1}. The difference trace between experimental and calculated spectra is included in the figure. The differences are largest in the region between maxima of the vibronic progressions, most likely a consequence of our neglect of low-frequency lattice modes. The maxima of the vibronic progressions are well-reproduced by our model. The difference trace reflects mainly the limitation to one vibrational mode, the assumption of harmonic potentials for the electronic states and the neglected coupling to energetically far A_{1g} states. Errors of the parameters resulting from the fit are smaller than 0.5%, but these errors again are influenced by the intrinsic model assumptions. A more realistic evaluation of the fit results is obtained by a comparison of the results for all three nickel(II) complexes. Our fit leads to parameter values very similar to those for $Ni(H_2O)_6^{2+}$. It is reassuring that distortions ΔQ_T identical to three significant digits are obtained for the A_{1g} and E_g levels arising from the triplet excited state, despite their treatment as independent parameters in our fit procedure. The coupling constant V_{ST} resulting from the fit varies by only 10% from the value used for $Ni(H_2O)_6^{2+}$, where it was not an adjustable parameter. The analysis for the tetragonal complex reveals therefore excited states with properties almost identical to the octahedral complex described in the preceding section. We note that the fit leads to small but nonzero values for μ_S and ΔQ_S, slightly different from $Ni(H_2O)_6^{2+}$. These differences could be caused by the assumption of one-dimensional potential energy surfaces for $NiCl_2(H_2O)_4$, a complex with two totally symmetric stretching modes involving aquo and chloro ligands.

$NiCl_6^{4-}$: D_{3d} Symmetry, One Singlet Coupled to Several Triplet States. The spectrum of $CsMgCl_3:Ni^{2+}$ in the region of interest is very similar in σ and π polarization, and we use only the σ polarization for the following analysis.[18,19] The electronic states in D_{3d} symmetry are shown in Scheme 1. Both the $^3A_{2g}$ and ^3E_g excited states have E_g spin−orbit levels that can interact with the $E_g(^1E_g)$ state. The splitting between the two triplet states is larger than 1000 cm^{-1}, determined experimentally from luminescence spectra arising from a higher excited state.[37] This system gives us the opportunity to examine the effects of three energetically different E_g levels of triplet parentage on the E_g level arising from ^1E_g. We make three separate calculations for the three sets of coupled E_g levels. The spectroscopic effects of coupling between E_g levels arising from the triplet states are negligible because the states have potential surfaces that are only displaced along the energy axis but not along Q_{a1g}. The partial spectra for the coupled E_g states and the total calculated spectrum are shown in Figure 5b, with the spectra involving the two closely spaced E_g states at lowest energy added together for clarity. The total calculated spectrum is in excellent agreement with the experiment. The difference trace again shows minimal differences in the region of the vibronic maxima and larger differences between maxima, most likely for the same reasons discussed for $NiCl_2(H_2O)_4$. We calculate a progression interval of 320 cm^{-1}, close to the experimental interval of 300 cm^{-1}. Adjustable parameters include the origins listed in Table 1, the vibrational frequency of the excited triplet states, the offsets ΔQ_S and ΔQ_T and the coupling constant V_{ST}. The energetic order of the $^3A_{2g}$ and ^3E_g states cannot be independently confirmed from the complicated excited-state spectra in this region.[37,38] The crystal field approach used for $NiCl_2(H_2O)_4$ is problematic for the hexachloride complexes because the crystal field potential appears to be significantly influenced by ions outside the first coordination sphere.[16] The energies of the triplet excited states resulting from our fit indicate that the ^3E_g state is lower than the $^3A_{2g}$ state, as summarized in Table 1.

(36) Press: W. H.; Teukolsky, S. A. *Comput. Phys.* **1991**, *5*, 426.
(37) May, P. S.; Güdel, H. U. *Chem. Phys. Lett.* **1989**, *164*, 612.
(38) May, P. S.; Güdel, H. U. *J. Lumin.* **1990**, *47*, 19.

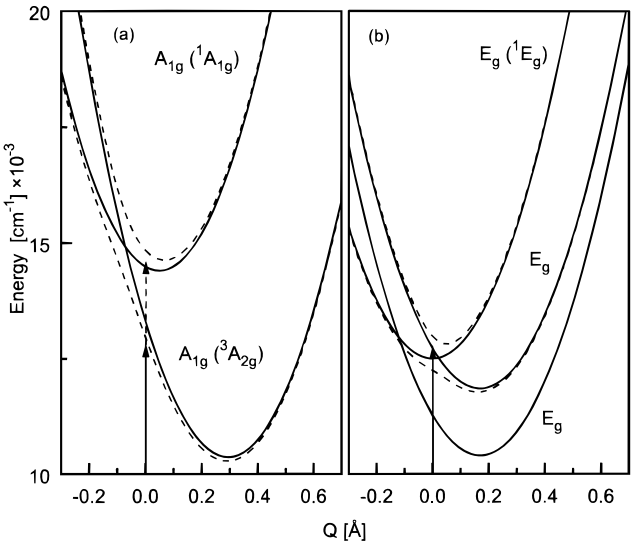

Figure 6. Potential energy diagrams for *trans*-$NiCl_2(H_2O)_4 \cdot 2H_2O$ (a) and $CsMgCl_3:Ni^{2+}$ (b). Diabatic and adiabatic potentials are shown as solid and dotted lines, respectively. Arrows denote Franck−Condon transitions from the ground state.

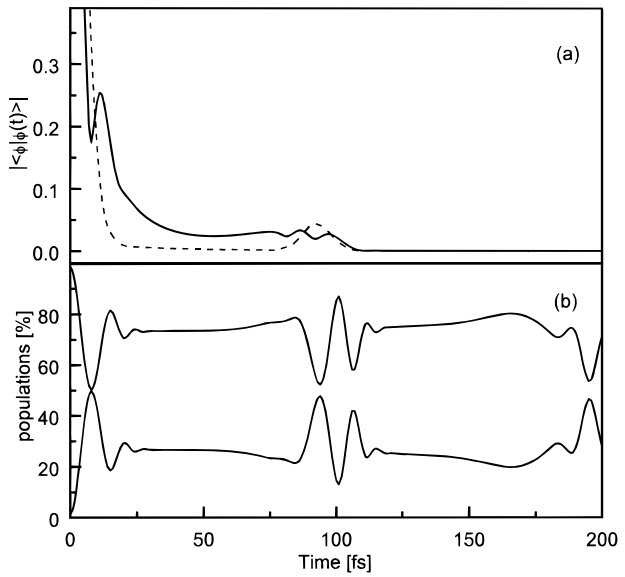

Figure 7. Absolute values of the autocorrelation (a) and time-dependent populations (b) of the coupled $A_{1g}(^1A_{1g})$ and A_{1g} ($^3A_{2g}$) excited states in Figure 6a for *trans*-$NiCl_2(H_2O)_4 \cdot 2H_2O$. Solid lines indicate calculations with the coupling constant V_{ST} in Table 1, dotted lines denote calculations with $V_{ST} = 0$.

The spectra for the sets of coupled E_g surfaces in Figure 5b show that energetically close levels of singlet and triplet parentage give rise to a band shape with two maxima of comparable intensity and a vibronic progression with a large spacing, whereas the band shape calculated for E_g states with a larger energy separation shows two unresolved bands of unequal intensity with the weaker transition attributed to the excited state with predominant singlet character. An experimental spectrum similar to the latter situation is reported for $CsCdCl_3:Ni^{2+}$,[39] where the triplet and singlet maxima are separated by 2000 cm^{-1} and only a weak, narrow band is observed on the high energy side of the broad spin allowed transition. This trend justifies the limitation of our spectroscopic model to pairs of coupled states that are energetically close. A large energy separation between levels of the same symmetry leads to very weak effects in the absorption spectra that cannot be easily observed experimentally.

Origin of the Large Energy Difference in the Intense Progression. Both the intensity and the vibronic structure of the spin-forbidden transition can be rationalized from the time-dependent wave function on the coupled potential energy surfaces obtained from the calculation of the spectra. We use the autocorrelation function and time dependent populations of the diabatic surfaces for $V_{ST} = 0$ and for the values of V_{ST} given in Table 1, and we neglect all levels with symmetries different from those of the coupled states. Figure 6 shows the coupled potentials for $NiCl_2(H_2O)_4$ and for $CsMgCl_3:Ni^{2+}$. The intersection of the singlet and triplet surfaces is close to the Franck−Condon region in both complexes. The absolute autocorrelation functions are shown in Figures 7a and 8a. The dotted curves for $V_{ST} = 0$ show an initial drop and a recurrence after one vibrational period. Two important changes occur for nonzero values of the coupling constant: a new maximum appears at very short times (10−30 fs), and the maximum corresponding to one vibrational period has a more complicated shape with its initial rise at a shorter time than calculated for $V_{ST} = 0$. These two effects lead to major changes of the band shape: the short time maximum corresponds to spectral intensity at energies higher by 2900 and 1080 cm^{-1} than the triplet origin for $NiCl_2(H_2O)_4$ and $CsMgCl_3:Ni^{2+}$, respectively. These energies correspond to the onsets of the intense progressions, again illustrating that their intensity is borrowed from the broad bands and a consequence of intersystem crossings. The shorter time of the first recurrence after one vibrational time period accounts for the larger separation of the members of the progression. We note that the larger spacing between the vibronic levels of the singlet excited states is qualitatively anticipated from the shape of the upper adiabatic potential surface. For nonzero coupling, this surface is narrower than the harmonic (diabatic) potential and a larger spacing of the energy levels is expected, but the adiabatic limit does not allow us to calculate band intensities for both the singlet and triplet states.

The autocorrelation for coupled states is strongly influenced by the transfer of wave packet amplitude between the two surfaces, as illustrated in Figures 7b, 8b, and 8c on the same time scale as used for the autocorrelation functions in Figures 7a and 8a. The wave packet amplitude is calculated by integrating ϕ_S and ϕ_T as defined in eq 3 for each point along the time axis. These time-dependent amplitudes or populations show a drop for the "allowed" surface at short times, followed by a back transfer of amplitude within 15 fs, leading to a new maximum of the autocorrelation. This transfer occurs initially when the wave packet moves through the crossing region and modulates the autocorrelation at short times, as illustrated by the comparison of the population and autocorrelation curves. The populations on the two surfaces remain approximately constant when the wave packet is far from the crossing region. Large changes occur again after one vibrational time period, when the time-dependent wave function is back near the crossing. These population changes lead to the complicated shape of the first recurrence in the autocorrelation of the coupled system and to the large spacing of the vibronic progression.

The time-dependent populations of the coupled states can also be used to examine the singlet and triplet assignments made for the title complexes. Figures 7b and 8c show that the average population of the triplet level is significantly higher than that of the singlet level, in intuitive agreement with the expectations for spin-allowed and spin-forbidden transitions. At certain times the populations can be equal or even inversed, a consequence

(39) May, P. S.; Güdel, H. U. *J. Lumin.* **1990**, *46*, 277.

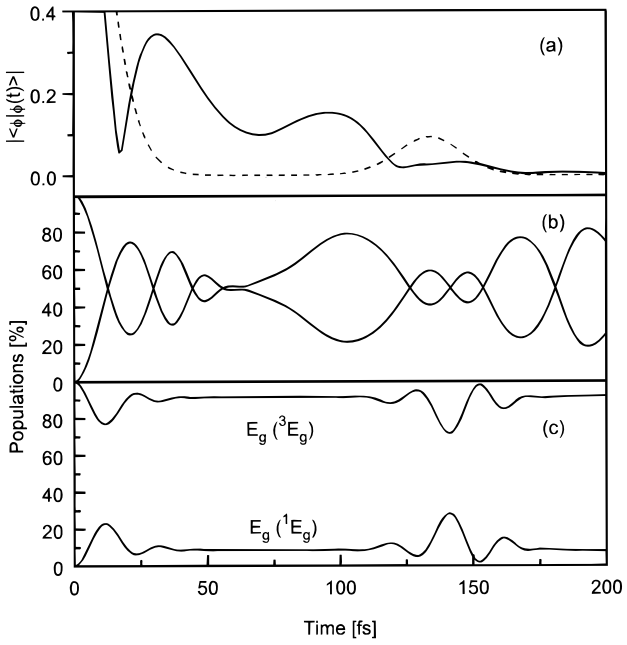

Figure 8. Absolute values of the autocorrelation (a) and time-dependent populations (b) of the energetically close pair of E_g excited states in Scheme 1 and Figure 6b for $CsMgCl_3:Ni^{2+}$. Solid lines indicate calculations with the coupling constant V_{ST} in Table 1, dotted lines denote calculations with $V_{ST} = 0$. The time-dependent populations for the coupled E_g states with a large energy separation are shown for comparison in panel c.

of the time-dependent wave function changing surfaces as it moves along Q_{a1g}, indicating the nonadiabatic behavior of the molecule in these interacting excited states and illustrating the difficulty of assigning singlet and triplet bands. Figure 8b shows the complicated crossover dynamics for states close in energy. The attribution of singlet and triplet character based on the time-dependent populations is impossible in this case, and physical and chemical properties of the singlet−triplet system cannot be determined separately for each state, illustrating the shortcomings of traditional spectroscopic assignments and of some analyses of photochemical reactivities.

Alternative Interpretations of the Band Shape. An alternative explanation of the double maximum observed in the room-temperature absorption spectrum of $Ni(H_2O)_6^{2+}$, where the high-frequency progression is not resolved, assigns the band shape to a Jahn−Teller effect in the $^3T_{1g}$ state with no spectroscopic evidence for the ^1E_g state.[11] The experimental observation of similar spectra for complexes with very different symmetries, presented in this work and in the literature,[6,8] and the absence of a significant Ham quenching of the electronic origins of the $^3T_{1g}$ band[8] provide clear experimental evidence against a strong Jahn−Teller effect in the $^3T_{1g}$ state. Only a strong Jahn−Teller effect involving a significant distortion along the normal coordinates of the active modes could account for the large splitting of the observed absorption band. A comprehensive study of these bands in a large series of complexes at room temperature indicates that a double maximum of the $^3T_{1g}/^1E_g$ band system is only observed for a narrow range of crystal field parameters between $0.8 < Dq/B < 1.1$.[6] Such a strong dependence of the Jahn−Teller distortions on Dq/B is not expected.

We note that the large vibronic spacing observed in the title compounds cannot be attributed to a missing mode effect (MIME), used to explain unusual spacings in a variety of transition metal complexes.[40,41] The MIME arises from excited-state distortions along multiple normal coordinates and cannot lead to progression intervals that are larger than the largest vibrational frequency involved,[40] as is the case for the title compounds.

A literature analysis of the absorption spectra of $NiCl_2$ and $NiBr_2$ proposes a two-phonon progression involving two quanta of the e_g vibration separating each member to account for the large progression interval.[10] The overall absorption spectra of these layered halides are very similar to those of $CsMgCl_3:Ni^{2+}$ and we compare the literature analysis to our model in the following. The experimental progression interval for $NiCl_2$ is 335 cm^{-1}.[10] The progression has five clearly discernible members and an intensity distribution similar to that of $CsMgCl_3:Ni^{2+}$, shown in Figure 5b. The point group of the $NiCl_6^{4-}$ unit is D_{3d}, but the distortion of the octahedral coordination sphere along the trigonal axis is a compression rather than an elongation as in $CsMgCl_3:Ni^{2+}$.[42,43] The vibrational frequencies of the a_{1g} and e_g modes of $NiCl_2$ are 269 and 173 cm^{-1}, respectively.[44] Progressions involving two quanta between each member are possible for non totally symmetric modes, such as the e_g vibration, based on symmetry arguments.[10] They are dominating the spectrum if the initial and final potential energy surfaces have different vibrational frequencies and if their minima are at exactly the same position along the normal coordinate. We examine a simple model of this situation based on the ground-state frequency for the e_g mode and an excited-state frequency of 167 cm^{-1}, corresponding to half the experimental spacing in the progression observed for $NiCl_2$. A calculation with these values leads to an intensity ratio of 1:0.0008 for the members of the progression involving 0 and 2 quanta of the e_g vibration, far from the ratio of 1:0.5 (±0.3) estimated from the experimental intensities of the intense progressions in Figures 2, 4, and 5. A displacement of the excited-state potential surface by just 0.01 Å along the e_g normal coordinate leads to a progression with its members separated by only *one* quantum of the vibrational energy, i.e., only half the observed interval. The intensity ratio of the first and second members of this progression is 1:0.009, an intensity for the second band higher by an order of magnitude than the two-quanta sideband observed for zero displacement. It is therefore not possible to quantitatively rationalize the intense vibronic progression in $NiCl_2$ and $CsMgCl_3:Ni^{2+}$ as a two-phonon progression in the e_g mode. The special case of a strong $e_g \times E_g(^1E_g)$ Jahn−Teller effect in these trigonal systems should lead to dramatically different spectra from those observed for tetragonal complexes such as $NiCl_2(H_2O)_4$, where the singlet excited states are no longer degenerate. We therefore conclude that the intense progression observed in several nickel halides arises from spin−orbit coupling between the singlet and triplet excited states, analogous to the situation for the $Ni(H_2O)_6^{2+}$ complex.

Conclusion

Our model rationalizes absorption band positions, intensities, and the unusual vibronic structure observed for a variety of nickel(II) compounds and underlines the important influence

(40) Tutt, L.; Zink, J. I. *J. Am. Chem. Soc.* **1986**, *108*, 5830.
(41) Preston, D. M.; Güntner, W.; Lechner, A.; Gliemann, G.; Zink, J. I. *J. Am. Chem. Soc.* **1988**, *110*, 5628.
(42) De Haan, Y. M. In *Molecular Dynamics and Structure*; Carter, R. S., Rush, J. J., Eds.; Natl. Bur. St. Spec. Publ. Vol. 301, Natl. Bur. Stand.: Washington, 1969; p 233.
(43) Achiwa, N. *J. Phys. Soc. Jpn.* **1969**, *27*, 561.
(44) Pollini, I.; Spinolo, G.; Benedek, G. *Phys. Rev.* **1980**, *B22*, 6369.

of intersystem crossings in these complexes. The physical origins of the observed spectroscopic effects can be identified from low-temperature, polarized single-crystal spectra and are qualitatively similar to those of interference dips and intensity borrowing.[45,46] Our experimental and calculated spectra illustrate that the intervals observed in vibronic progressions can depend on interactions between different electronic states, an effect that has traditionally been neglected.

Acknowledgment. This work was made possible by research grants from the NSERC (Canada). We thank Hans U. Güdel for allowing us to use the absorption spectrum of $CsMgCl_3$:Ni^{2+}, measured by C.R. in his laboratory.

JA9740733

(45) Reber, C.; Zink, J. I. *J. Chem. Phys.* **1992**, *96*, 2681.
(46) Wexler, D.; Zink, J. I.; Reber, C. *J. Phys. Chem.* **1992**, *96*, 8757.